NASA TECHNICAL MEMORANDUM

NASA TM X-2713

NASA TM X-2713

LONGITUDINAL AERODYNAMIC PERFORMANCE OF A SERIES OF POWER-LAW AND MINIMUM-WAVE-DRAG BODIES AT MACH 6 AND SEVERAL REYNOLDS NUMBERS

by George C. Ashby, Jr.

Langley Research Center
Hampton, Va. 23665

NATIONAL AERONAUTICS AND SPACE ADMINISTRATION • WASHINGTON, D. C. • AUGUST 1974

1. Report No. NASA TM X-2713	2. Government Accession No.	3. Recipient's Catalog No.
4. Title and Subtitle LONGITUDINAL AERODYNAMIC PERFORMANCE OF A SERIES OF POWER-LAW AND MINIMUM-WAVE-DRAG BODIES AT MACH 6 AND SEVERAL REYNOLDS NUMBERS		5. Report Date August 1974 6. Performing Organization Code
7. Author(s) George C. Ashby, Jr.		8. Performing Organization Report No. L-7609
9. Performing Organization Name and Address NASA Langley Research Center Hampton, Va. 23665		10. Work Unit No. 117-07-01-01 11. Contract or Grant No.
12. Sponsoring Agency Name and Address National Aeronautics and Space Administration Washington, D.C. 20546		13. Type of Report and Period Covered Technical Memorandum 14. Sponsoring Agency Code

15. Supplementary Notes

16. Abstract

Experimental data have been obtained for two series of bodies at Mach 6 and Reynolds numbers, based on model length, from 1.4×10^6 to 9.5×10^6. One series consisted of axisymmetric power-law bodies geometrically constrained for constant length and base diameter with values of the exponent n of 0.25, 0.5, 0.6, 0.667, 0.75, and 1.0. The other series consisted of positively and negatively cambered bodies of polygonal cross section, each having a constant longitudinal area distribution conforming to that required for minimizing zero-lift wave drag at hypersonic speeds under the geometric constraints of given length and volume.

At the highest Reynolds number, the power-law body for minimum drag is blunter (exponent n lower) than predicted by inviscid theory ($n \approx 0.6$ instead of $n = 0.667$); however, the peak value of lift-drag ratio occurs at $n = 0.667$. Viscous effects were present on the bodies of polygonal cross section but were less pronounced than those on the power-law bodies. The trapezoidal bodies with maximum width at the bottom were found to have the highest maximum lift-drag ratio and the lowest minimum drag.

17. Key Words (Suggested by Author(s))	18. Distribution Statement
Hypersonic flow Minimum drag Boundary layer	Unclassified – Unlimited STAR Category 01

19. Security Classif. (of this report)	20. Security Classif. (of this page)	21. No. of Pages	22. Price*
Unclassified	Unclassified	27	$3.25

*For sale by the National Technical Information Service, Springfield, Virginia 22151

LONGITUDINAL AERODYNAMIC PERFORMANCE OF A SERIES OF POWER-LAW AND MINIMUM-WAVE-DRAG BODIES AT MACH 6 AND SEVERAL REYNOLDS NUMBERS

By George C. Ashby, Jr.
Langley Research Center

SUMMARY

Experimental data have been obtained for two series of bodies at Mach 6 and Reynolds numbers, based on model length, from 1.4×10^6 to 9.5×10^6. One series consisted of axisymmetric power-law bodies geometrically constrained for constant length and base diameter with values of the exponent n of 0.25, 0.5, 0.6, 0.667, 0.75, and 1.0. The other series consisted of positively and negatively cambered bodies of polygonal cross section, each having a constant longitudinal area distribution conforming to that required for minimizing zero-lift wave drag at hypersonic speeds under the geometric constraints of given length and volume.

At the highest Reynolds number, the power-law body for minimum drag is blunter (exponent n lower) than predicted by inviscid theory ($n \approx 0.6$ instead of $n = 0.667$); however, the peak value of lift-drag ratio occurs at $n = 0.667$. Viscous effects were present on the bodies of polygonal cross section but were less pronounced than those on the power-law bodies. The trapezoidal bodies with maximum width at the bottom were found to have the highest maximum lift-drag ratio and the lowest minimum drag.

INTRODUCTION

Many basic studies, typified by the results presented in references 1 and 2, have been made to determine the longitudinal cross-sectional area distribution and cross-sectional shape of bodies having zero-lift pressure drag at hypersonic speed. The results of such studies have been shown in references 3 and 4 to apply to lifting reentry bodies. More recently, with the focus of interest on advanced (for example, the space shuttles) systems for transportation to and from earth orbit, a critical assessment of the validity and practical value of past solutions for optimum shapes was presented in reference 5. For that assessment, a portion of the experimental data was obtained for two series of bodies at Mach 6, angles of attack extending beyond that for maximum lift-drag ratio, and several Reynolds numbers. The first series consisted of axisymmetric power-law bodies

of revolution geometrically constrained for constant length and base diameter. The second series consisted of positively and negatively cambered bodies of polygonal cross section, similar to those of reference 4, each having the same longitudinal area distribution required for minimizing wave drag at hypersonic speeds. The data show some major viscous effects, especially for the power-law bodies; however, in reference 5 only the data for minimum drag and maximum lift-drag ratio were utilized. The viscous effects on the minimum drag of the power-law bodies resulting from boundary-layer transition were analyzed and discussed in reference 6.

Because of the interest in the data for such basic bodies, this paper presents the complete longitudinal aerodynamic characteristics obtained on these power-law and polygonal bodies at Mach 6 with the effects of Reynolds number indicated. The data were obtained in the Langley 20-inch Mach 6 tunnel at Reynolds numbers (based on model length) from 1.4×10^6 to 9.5×10^6 and at angles of attack from -8° to 16°.

SYMBOLS

The longitudinal aerodynamic characteristics of the bodies are referenced to the stability-axis system. The moment coefficients are referenced to the 66.67 percent body station for the power-law bodies; whereas the moment coefficients for the polygonal bodies are referenced to the 55 percent body station to be compatible with the data of reference 4.

A_b model base area, meters^2

C_D drag coefficient, $\frac{\text{Drag}}{qA_b}$

C_L lift coefficient, $\frac{\text{Lift}}{qA_b}$

C_m pitching-moment coefficient about specified reference point, $\frac{\text{Pitching moment}}{qA_b l}$

l model length, cm

L/D lift-drag ratio

n exponent in shape equation $\frac{r}{R} = \left(\frac{x}{l}\right)^n$ for power-law bodies

$N = \pi\left(\frac{\text{Span}}{\text{Height}}\right)$ for polygonal family

q dynamic pressure, newtons/meter^2

r,x coordinates on meridian curve of power-law body
(x = Axial distance from nose; r = Radius at station x)

R base radius of power-law bodies, cm

$R_{\infty,l}$ Reynolds number, based on free-stream conditions and body length

x_{cp} distance to center of pressure measured from nose, cm

α angle of attack, deg

Subscripts:

$(L/D)_{max}$ at maximum lift-drag ratio

max maximum

min minimum

o at zero lift

APPARATUS AND METHODS

Models

Sketches of the models used in the investigation are shown in figures 1 and 2 and their coordinates are listed in tables I and II. The six power-law bodies, n = 0.25, 0.5, 0.6, 0.667, 0.75, and 1.0, were circular in cross section, had a fineness ratio of 6.63, and were constrained for constant length and base diameter. The polygonal bodies had the same longitudinal cross-sectional area distribution as a zero-lift minimum-wave-drag body constrained for length and volume as determined in references 1 and 7. Seven models were constructed for this group: two with a triangular cross section, two with trapezoidal cross section having the ratio of the parallel sides of 1 to 3, two with

trapezoidal cross section having the ratio of the parallel sides of 2 to 3, and one with a rectangular cross section. One model of each cross-sectional pair had the narrow surface cambered and the wide surface flat; whereas the other model of each pair had the wide surface cambered and the narrow surface flat. These bodies had an effective fineness ratio of 5 based on an equivalent diameter for the base area. Bodies 2, 4, 5, 6, and 7 were longer than bodies 1 and 3 (see table II) because of the forward cross-sectional area required to accommodate a specific set of strain-gage balances.

Wind Tunnel and Tests

The tests were conducted in the Langley 20-inch Mach 6 tunnel in air. The tunnel is a blowdown type exhausting to either atmosphere or vacuum with an operating range of stagnation pressures from 3 to 35 atmospheres (3.04×10^5 to 35.5×10^5 N/m^2) and stagnation temperatures up to 589 K. The general details of the tunnel, along with schematic drawings, are presented in reference 8. The Reynolds number range of the present test, based on model length, was from 1.4×10^6 to 9.5×10^6. Test angle of attack for the power-law bodies was from -4° to 16° and for the trapezoidal bodies from -8° to 16°.

Methods

The aerodynamic forces and moments were measured by an internally mounted, sting-supported, water-cooled, six-component strain-gage balance. The model angle of attack was determined by reflecting a light beam from a combination lens and right-angle prism embedded in each model onto a calibrated screen. For the power-law bodies, base pressure measurements were made with six uniformly spaced tubes and for the polygonal bodies, with three uniformly spaced tubes. At zero angle of attack the measured pressures were uniform over the base (varying within the 1/4 percent of full-scale range of the transducer). At finite angle of attack, aerodynamically symmetrical pairs of tubes were also in good agreement. The average of the measurements was used to adjust the axial-force coefficient to the conditions for free-stream static pressure on the base. Most of the $(L/D)_{max}$ values faired through or plotted in figures 3 to 6 were determined by a computer program which fits a fifth-order polynomial to the drag polar and determines $(L/D)_{max}$ from the tangent line through the origin. Mach number was measured for each test point with a total-pressure probe and varied from 5.86 to 6.02.

Accuracy

On the basis of balance calibrations, read-out accuracy, and dynamic-pressure accuracy, the data presented are estimated to be accurate within the following limits:

$R_{\infty,l}$	C_D	C_L	C_m	L/D
Power-law bodies				
1.50×10^6	±0.0106	±0.028	±0.0040	±0.842
4.37	±.0037	±.010	±.0017	±.294
6.42	±.0025	±.007	±.0012	±.201
9.50	±.0019	±.005	±.0009	±.152
Polygonal bodies				
1.4×10^6	±0.0084	±0.022	±0.0040	±0.335
3.7	±.0029	±.008	±.0016	±.316
4.8	±.0025	±.006	±.0013	±.215
5.6	±.0020	±.005	±.0011	±.080
7.4	±.0015	±.004	±.0009	±.062

Angle of attack is estimated to be accurate within $\pm 0.1^\circ$ and Mach number is estimated to be accurate within ±0.02.

RESULTS AND DISCUSSION

Power-Law Bodies

The longitudinal aerodynamic performance data for the six power-law bodies over the Reynolds number range are presented in figure 3. The data for Reynolds number 1.5×10^6 are faired with a dashed line because they were limited to three angles of attack. Only the parameters involved with drag $(C_D$ and $L/D)$ are significantly affected by Reynolds number. The lift and pitch are slightly affected but, in general, only at angles of attack above 8°. Reynolds number effects on drag and performance are significant for all bodies from $n = 0.5$ to 1.0. These effects are related to changes in body bluntness which decreases significantly for values of n between 0.25 and 0.5; whereas, from $n = 0.5$ to 1.0, only slight changes in bluntness are noted, since those bodies are relatively slender. (See fig. 1.) These effects can more readily be seen in figure 4 where summary plots of the pertinent aerodynamic parameters from figure 3 are presented. The drag coefficients are seen in figure 4 to be a minimum near $n = 0.6$ for the higher Reynolds numbers instead of at $n = 0.667$ which was predicted for inviscid flow in reference 5. The cause of the variation with Reynolds number is indicated in reference 6 to result from boundary-layer-transition effects. In reference 6, drag calculated for each body at zero angle of attack by using the measured locations of boundary-layer transition and including the effect of boundary-layer displacement on both skin friction

and wave drag show the same trends as the experimental data of figure 4. From figure 4 it is noted that at Reynolds numbers from 4.4×10^6 to 9.5×10^6 the n value for $(L/D)_{max}$ (approximately 0.667) is generally larger than the n value for minimum drag (approximately 0.6). However, the values of $(L/D)_{max}$ are relatively constant for n between 0.6 and 0.75, and the change in $(L/D)_{max}$ is slight. The effect of boundary-layer transition on drag observed at zero angle of attack apparently does not occur at the angle of attack for $(L/D)_{max}$ ($\alpha = 6^o$ to 7^o).

Polygonal Bodies

The longitudinal aerodynamics for the seven polygonal bodies over the Reynolds number range are presented in figure 5. A summary plot of pertinent aerodynamic parameters from figure 5 is presented in figure 6 as a function of the span to height parameter N for the four Reynolds numbers of the investigation. This parameter was used here for convenience of plotting the data and is consistent with the data from reference 5. Both positive and negative camber results were obtained from the data of figure 5. The models were mounted in the positive camber orientation for the tests; therefore, the data obtained at negative angles of attack correspond to that for negative camber at positive angles of attack.

The bodies of rectangular and trapezoidal cross section with positive camber and maximum span on the bottom have higher $(L/D)_{max}$ than the corresponding bodies with maximum span on the top. Similar results were shown in reference 5 for Mach numbers 10.4 and 20. The same general conclusion was reached in reference 4 at Mach number 10 and a Reynolds number of 1.4×10^6 except the triangular cross section was found to have the highest $(L/D)_{max}$. This disagreement was traced to the difference in drag for the two sets of data. In the present tests the minimum drag was higher for the triangular body than for the other bodies; whereas in reference 4 the minimum drag is nearly constant for all the bodies. Although the negative camber body has somewhat lower $(L/D)_{max}$ than the positive camber body, its positive $C_{m,o}$ makes it desirable from consideration of trim and stability, as previously pointed out in reference 4.

Reynolds number effects are not as pronounced for the polygonal bodies as for the power-law bodies. Several factors tend to suppress the variation of total drag with Reynolds number for these bodies. For example, the differences in viscous effects between the two sets of bodies can be partly attributed to the differences in their geometric shapes. The power-law bodies are bodies of revolution; therefore, at $C_{D,min}$ ($\alpha = 0^o$), the theoretical skin-friction distribution along each meridian is the same. The polygonal bodies, however, are asymmetric and should have different transition locations on the various surfaces at $C_{D,min}$ ($\alpha \neq 0^o$) and, therefore, different skin-friction distributions along each surface. Furthermore, for the polygonal bodies, minimum drag

does not occur at zero angle of attack; and in most cases the minimum drag does not occur at a test point. The variation of drag with Reynolds number is, therefore, influenced somewhat by the manner of fairing the curves of C_D as a function of α. Finally, at the lowest test Reynolds number, the minimum drag was only definable for bodies 3, 4, 6, and 7 because of the test limits on the angle of attack.

The minimum drag for body 7 was slightly higher than that of the other bodies at Reynolds number 1.4×10^6. Data for Mach 10.4 and Reynolds number 1.4×10^6 were obtained by using these same models and show similar results. It is also noted in figure 6 at Reynolds number 3.7×10^6 and above, that although the $(L/D)_{max}$ and $C_{D,min}$ are at different angles of attack, they vary inversely; that is, increasing $C_{D,min}$ results in decreasing $(L/D)_{max}$.

CONCLUDING REMARKS

Experimental data have been obtained for two series of bodies at Mach 6 and Reynolds numbers, based on model length, from 1.4×10^6 to 9.5×10^6. One series was axisymmetric power-law bodies geometrically constrained for constant length and base diameter with values of the exponent n in the shape equation of 0.25, 0.5, 0.6, 0.667, 0.75, and 1.0. The other series consisted of positively and negatively cambered polygonal bodies, each having the same longitudinal area distribution that is required for minimizing wave drag at hypersonic speeds.

Reynolds number effects on drag and performance are significant for the power-law bodies from $n = 0.5$ to 1.0. At the higher Reynolds number the variation of boundary-layer transition location with nose bluntness causes the drag to be a minimum for the $n \approx 0.6$ body instead of the $n = 0.667$ body, which has been predicted to have minimum drag in inviscid flow.

Viscous effects were present on the polygonal bodies but were less pronounced than those on the power-law bodies. The bodies of trapezoidal cross section with maximum width at the bottom were found to have the highest maximum lift-drag ratio and the lowest minimum drag rather than the bodies of triangular cross section. This result is consistent with other experimental results at Mach numbers 10.4 and 20. Although the negatively cambered bodies had somewhat lower maximum lift-drag ratio than the positively cambered bodies, their lower corresponding angle of attack and positive moment at zero lift make than desirable for practical applications from trim and stability considerations.

Langley Research Center,
National Aeronautics and Space Administration,
Hampton, Va., May 23, 1974.

REFERENCES

1. Eggers, A. J., Jr.; Resnikoff, Meyer M.; and Dennis, David H.: Bodies of Revolution Having Minimum Drag at High Supersonic Airspeeds. NACA Rep. 1306, 1957. (Supersedes NACA TN 3666.)

2. Miele, Angelo: Slender Shapes of Minimum Drag in Newtonian Flow. Z. Flugwissenschaften, Jahrg. 11, Heft 5, May 1963, pp. 203-210.

3. Spencer, Bernard, Jr.; and Fox, Charles H., Jr.: Hypersonic Aerodynamic Performance of Minimum-Wave-Drag Bodies. NASA TR R-250, 1966.

4. Spencer, Bernard, Jr.: Hypersonic Aerodynamic Characteristics of Minimum-Wave-Drag Bodies Having Variations in Cross-Sectional Shape. NASA TN D-4079, 1967.

5. Love, E. S.: Design of Bodies for Low Drag and High Performance in Practical Hypersonic Flight. Performance and Dynamics of Aerospace Vehicles, NASA SP-258, 1971, pp. 103-174.

6. Ashby, George C., Jr.; and Harris, Julius E.: Boundary-Layer Transition and Displacement-Thickness Effects on Zero-Lift Drag of a Series of Power-Law Bodies at Mach 6. NASA TN D-7723, 1974.

7. Miele, Angelo: Similarity Laws for Optimum Hypersonic Bodies. Astronaut. Acta, vol. II, no. 3, 1965, pp. 202-206.

8. Goldberg, Theodore J.; and Hefner, Jerry N. (With appendix by James C. Emery): Starting Phenomena for Hypersonic Inlets With Thick Turbulent Boundary Layers at Mach 6. NASA TN D-6280, 1971.

TABLE I.- COORDINATES FOR POWER-LAW BODIES

$$\left[\frac{r}{R} = \left(\frac{x}{l}\right)^n\right]$$

n = 0.25		n = 0.5		n = 0.6		n = 0.667		n = 0.75		n = 1.0	
x/l	r/R	x/l	r/R	x/l	r/R	x/l	r/R	x/l	r/R	x/l	r/R
0.0007	0.076	0.0007	0.054	0.0007	0.029	0.0007	0.020	0.0007	0.010	0.0007	0.017
.001	.117	.001	.060	.001	.037	.001	.026	.001	.012	.001	.018
.002	.142	.002	.071	.002	.042	.002	.029	.002	.015	.002	.019
.003	.160	.003	.078	.003	.046	.003	.030	.003	.018	.003	.020
.004	.180	.004	.085	.004	.051	.004	.033	.004	.021	.004	.021
.009	.258	.009	.110	.009	.070	.009	.048	.009	.035	.009	.027
.014	.309	.014	.127	.014	.077	.014	.061	.014	.050	.014	.031
.036	.422	.036	.186	.036	.144	.036	.110	.036	.097	.036	.051
.054	.471	.054	.227	.054	.183	.054	.146	.054	.129	.054	.068
.071	.509	.071	.264	.071	.217	.071	.177	.071	.154	.071	.082
.214	.669	.214	.471	.214	.397	.214	.363	.214	.326	.214	.221
.357	.764	.357	.610	.357	.540	.357	.510	.357	.472	.357	.363
.571	.872	.571	.768	.571	.730	.571	.703	.571	.677	.571	.578
.714	.928	.714	.859	.714	.830	.714	.811	.714	.798	.714	.721
.857	.970	.857	.940	.857	.924	.857	.910	.857	.914	.857	.866
1.004	1.003	1.001	1.002	1.001	.996	.997	1.002	.984	1.007	.999	1.008

TABLE II.- POLYGONAL-BODY COORDINATES

		N = 4		N = 5.333		N = 6.667		N = 8	
		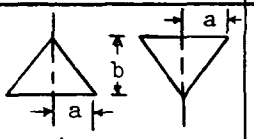		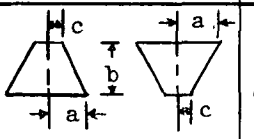		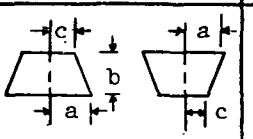		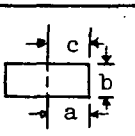	
		Body 1	Body 2	Body 3	Body 4	Body 5	Body 6	Body 7	
x/l	a/l	b/l		b/l	c/l	b/l	c/l	b/l	c/l
0	0	0		0	0	0	0	0	0
.006	.0042	.0067		.0050	.0014	.0040	.0028	.0033	.0042
.008	.0047	.0074		.0055	.0016	.0044	.0031	.0037	.0047
.010	.0063	.0099		.0074	.0021	.0060	.0042	.0050	.0063
.015	.0077	.0122		.0091	.0026	.0073	.0052	.0061	.0077
.020	.0095	.0149		.0112	.0032	.0089	.0063	.0074	.0095
.030	.0129	.0202		.0152	.0043	.0121	.0086	.0101	.0129
.040	.0161	.0253		.0190	.0054	.0152	.0108	.0127	.0161
.050	.0190	.0299		.0224	.0063	.0179	.0127	.0149	.0190
.060	.0219	.0343		.0258	.0073	.0206	.0146	.0172	.0219
.070	.0245	.0385		.0289	.0082	.0231	.0163	.0192	.0245
.080	.0270	.0424		.0318	.0090	.0255	.0180	.0212	.0270
.090	.0297	.0466		.0349	.0099	.0280	.0198	.0233	.0297
.100	.0320	.0503		.0377	.0107	.0302	.0213	.0251	.0320
.120	.0370	.0581		.0436	.0123	.0349	.0247	.0291	.0370
.140	.0411	.0646		.0484	.0137	.0387	.0274	.0323	.0411
.160	.0453	.0711		.0533	.0151	.0427	.0302	.0356	.0453
.200	.0534	.0839		.0629	.0178	.0503	.0356	.0419	.0534
.240	.0607	.0953		.0715	.0202	.0572	.0404	.0476	.0607
.280	.0677	.1063		.0797	.0226	.0638	.0451	.0532	.0677
.320	.0741	.1164		.0873	.0247	.0698	.0494	.0582	.0741
.360	.0803	.1262		.0946	.0268	.0757	.0535	.0631	.0803
.400	.0861	.1353		.1015	.0287	.0812	.0574	.0677	.0861
.440	.0920	.1445		.1084	.0307	.0867	.0613	.0722	.0920
.480	.0975	.1531		.1148	.0325	.0919	.0650	.0766	.0975
.520	.1029	.1616		.1212	.0343	.0969	.0686	.0808	.1029
.580	.1100	.1728		.1296	.0367	.1037	.0733	.0864	.1100
.660	.1187	.1864		.1398	.0396	.1118	.0791	.0932	.1187
.720	.1245	.1956		.1467	.0415	.1173	.0830	.0978	.1245
.780	.1296	.2036		.1527	.0432	.1222	.0864	.1018	.1296
.840	.1342	.2107		.1581	.0447	.1265	.0894	.1054	.1342
.900	.1379	.2166		.1625	.0460	.1300	.0919	.1083	.1379
.920	.1390	.2181		.1636	.0463	.1309	.0926	.1091	.1390
.940	.1398	.2195		.1646	.0466	.1317	.0932	.1098	.1398
.960	.1405	.2207		.1655	.0468	.1324	.0937	.1104	.1405
.970	.1408	.2212		.1659	.0469	.1328	.0939	.1106	.1408
.980	.1411	.2216		.1662	.0470	.1330	.0941	.1108	.1411
.990	.1413	.2219		.1664	.0471	.1332	.0942	.1110	.1413
1.000	.1414	.2221		.1666	.0471	.1333	.0943	.1111	.1414
Length, l, cm		25.4	30.48	25.4	30.48	30.48	30.48	30.48	30.48

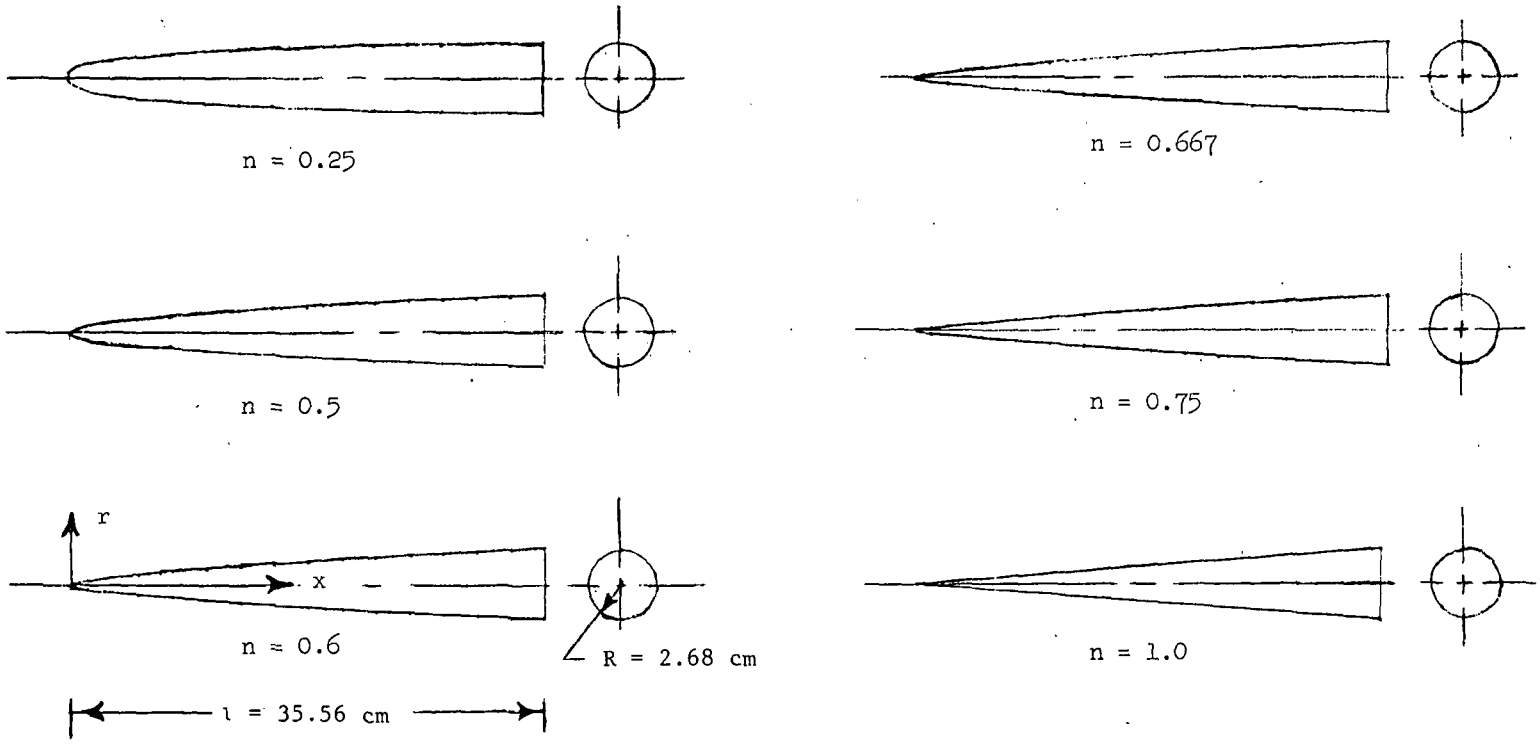

Figure 1.- Power-law bodies tested. Model shape equation: $\frac{r}{R} = \left(\frac{x}{l}\right)^n$. Coordinates are in table I.

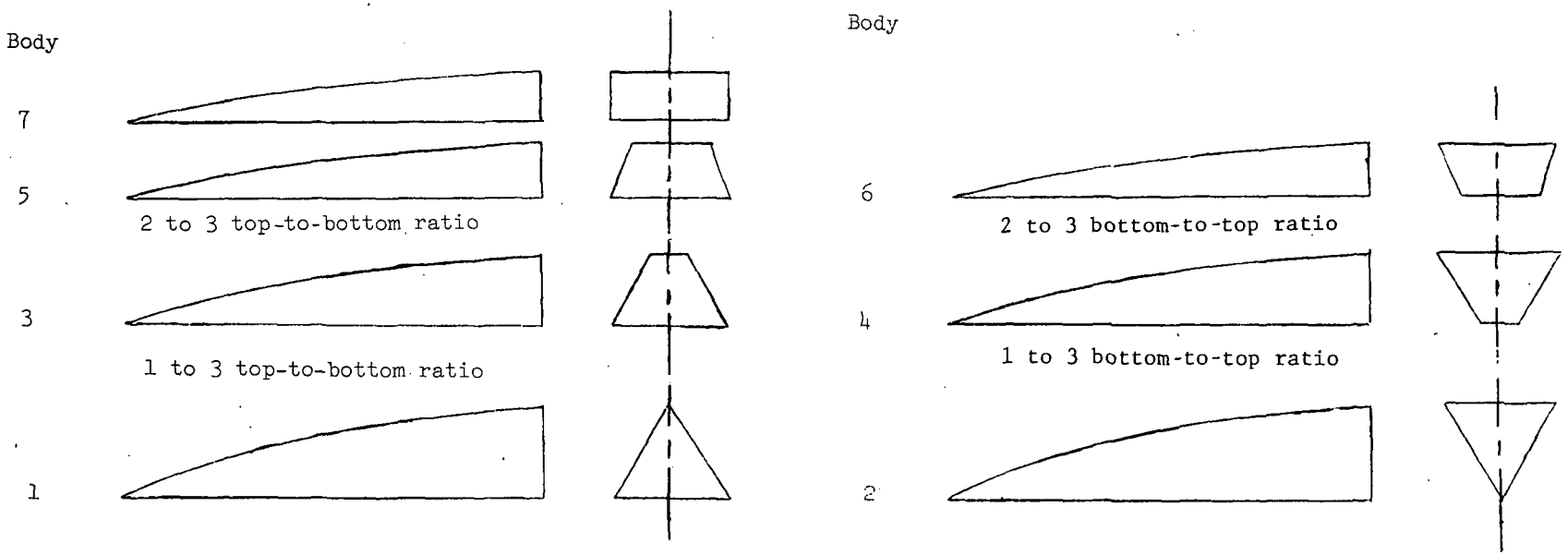

Figure 2.- Polygonal bodies tested (positive camber orientation shown). Coordinates are in table II. Bodies 1 and 3 were 25.4 centimeters long and other bodies were 30.48 centimeters long.

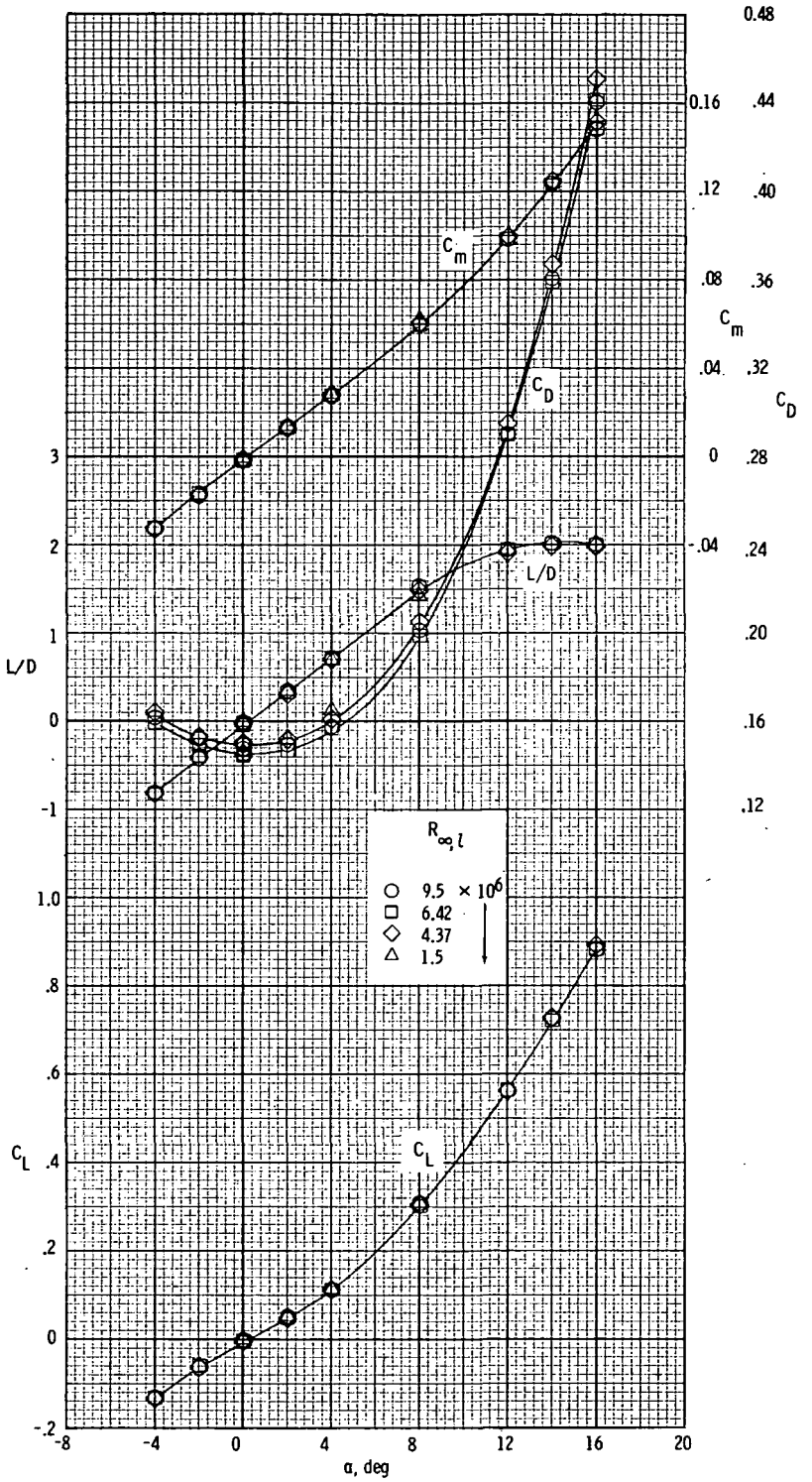

(a) n = 0.25.

Figure 3.- Longitudinal aerodynamic characteristics of power-law bodies at Mach number 6 and several Reynolds numbers.

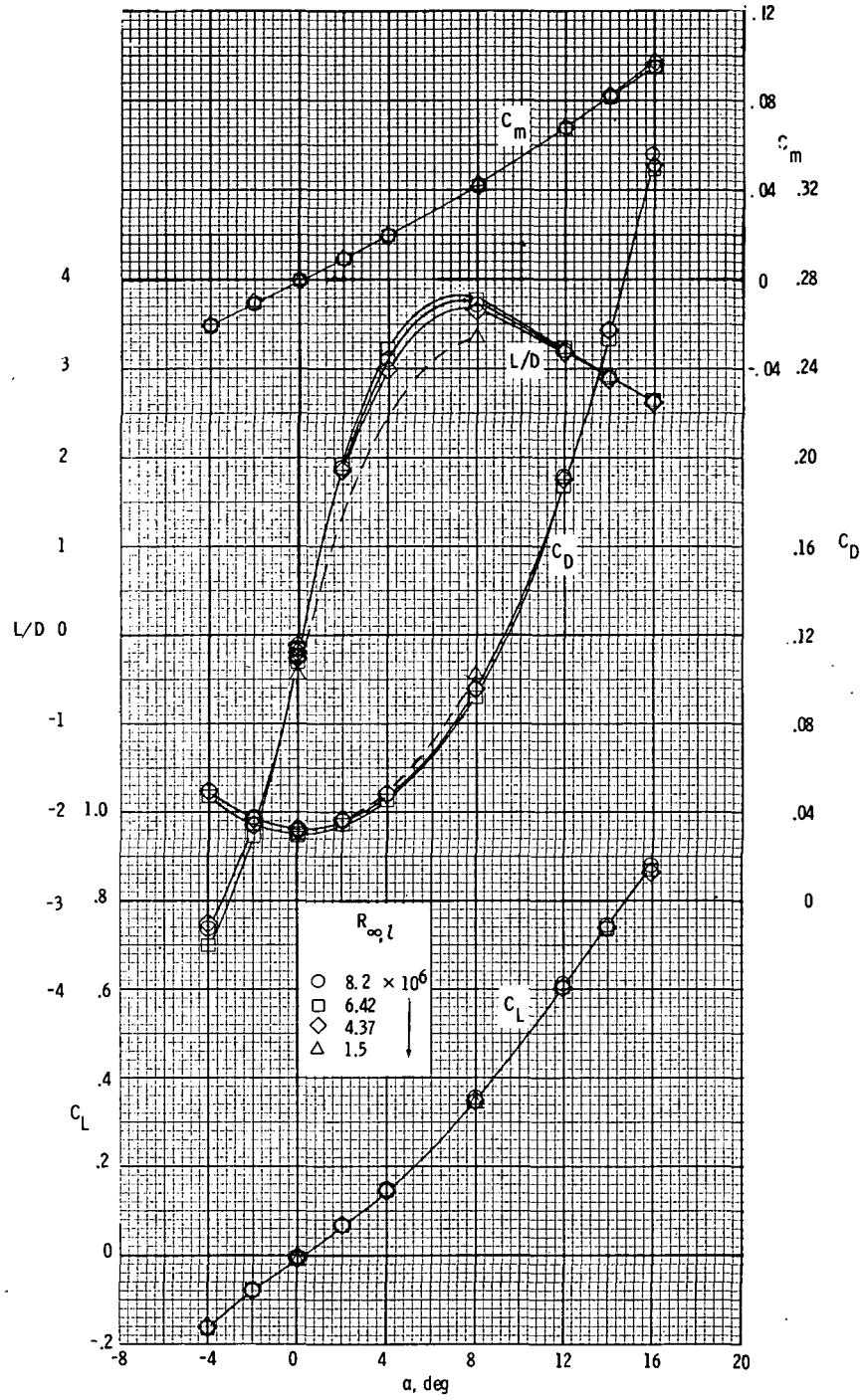

(b) n = 0.5.

Figure 3.- Continued.

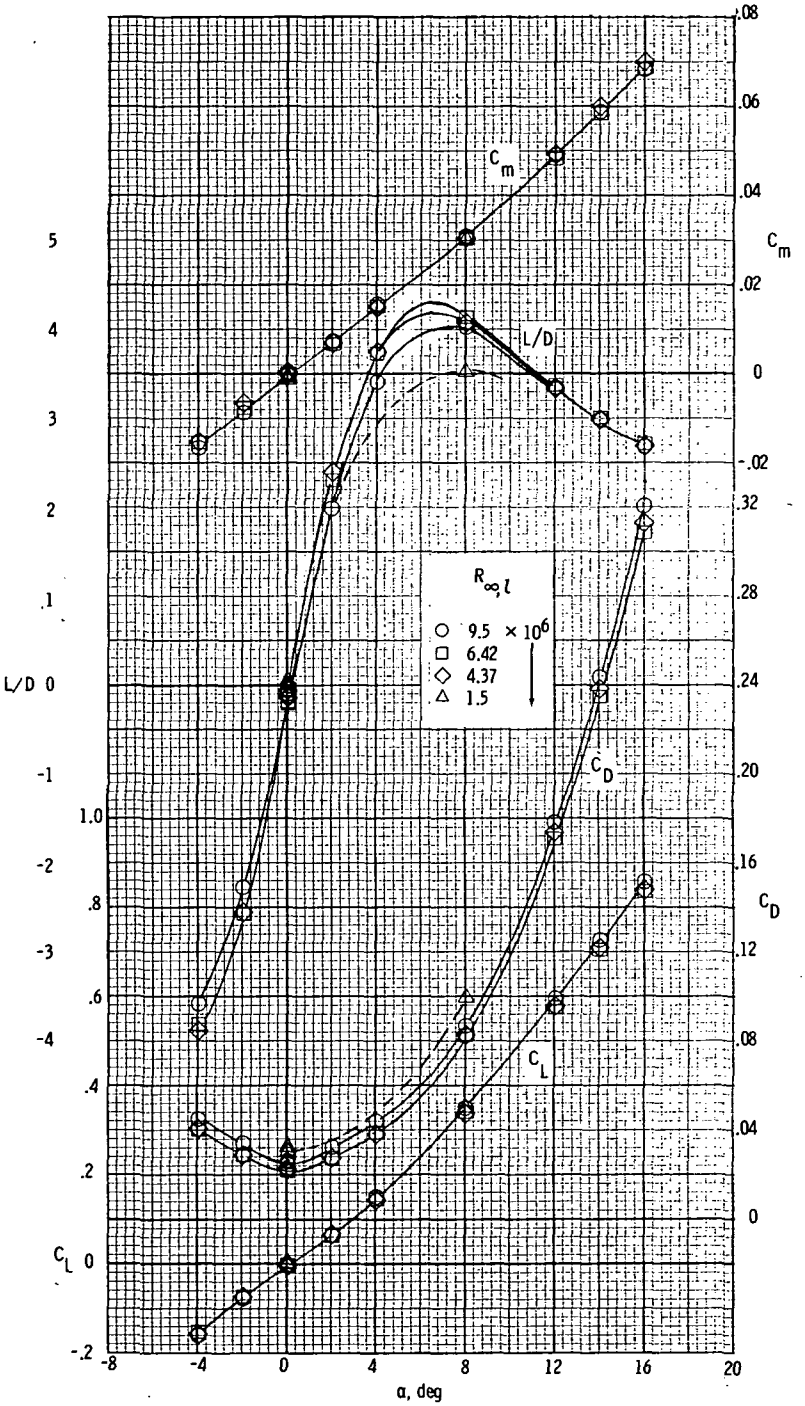

(c) n = 0.6.

Figure 3.- Continued.

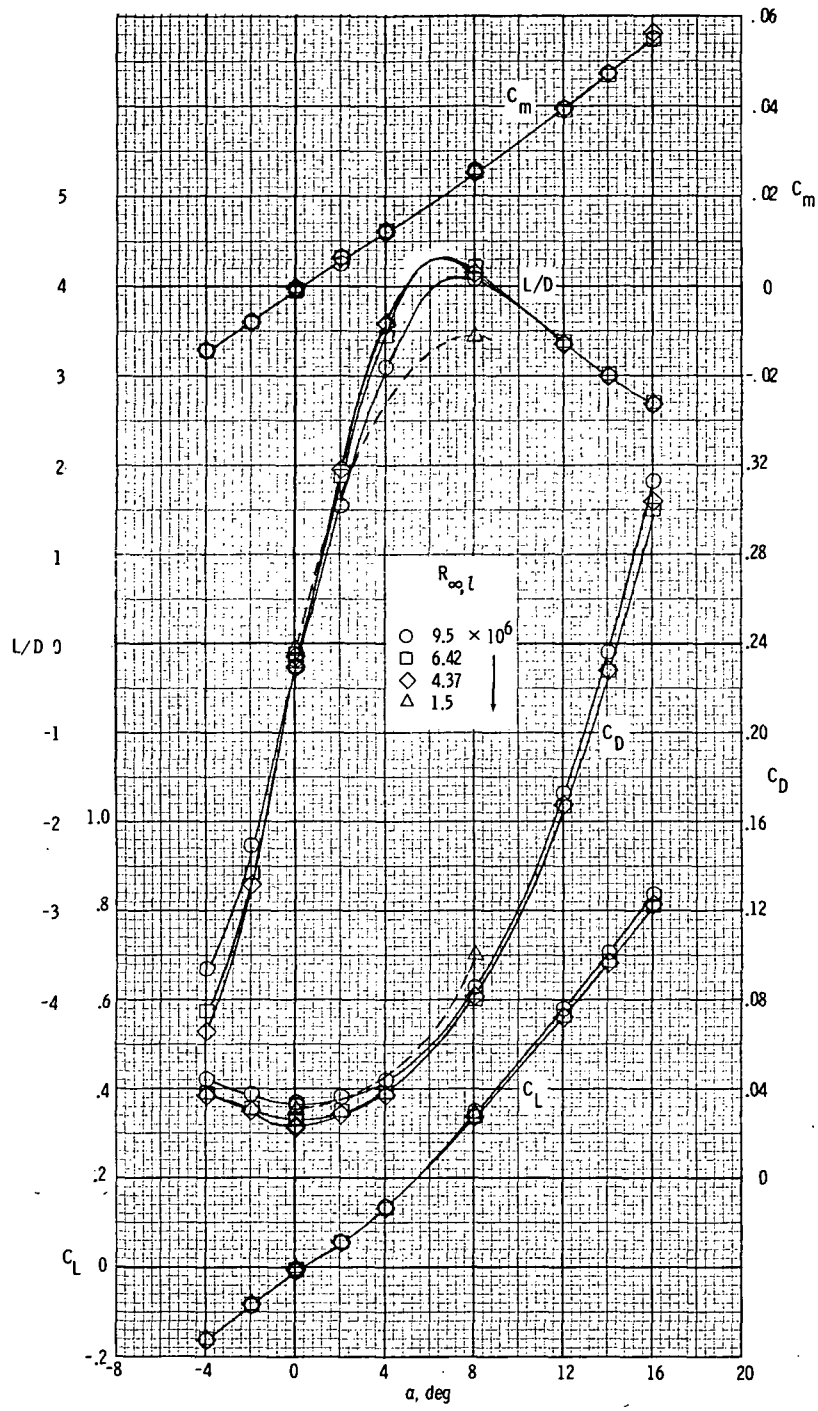

(d) n = 0.667.

Figure 3.- Continued.

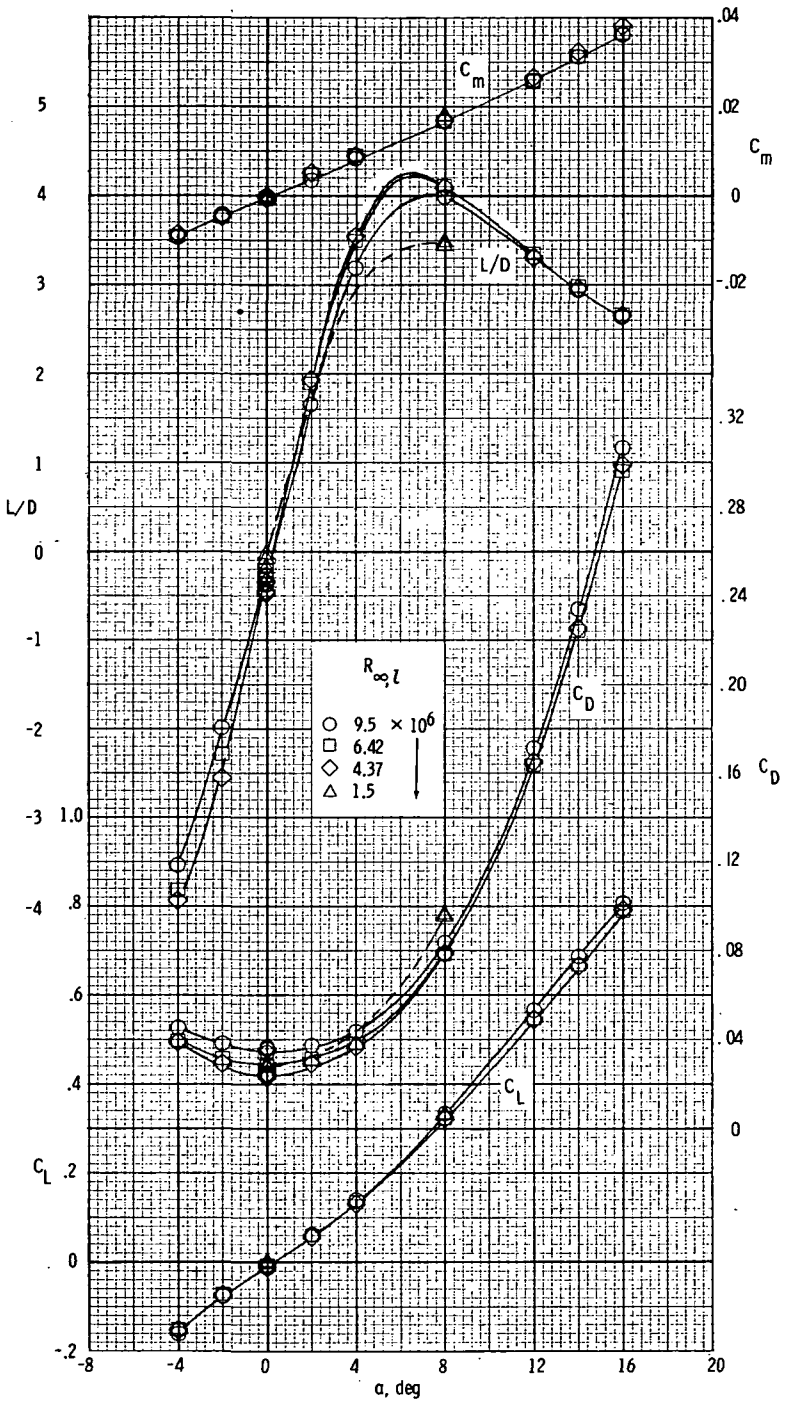

(e) n = 0.75.

Figure 3.- Continued.

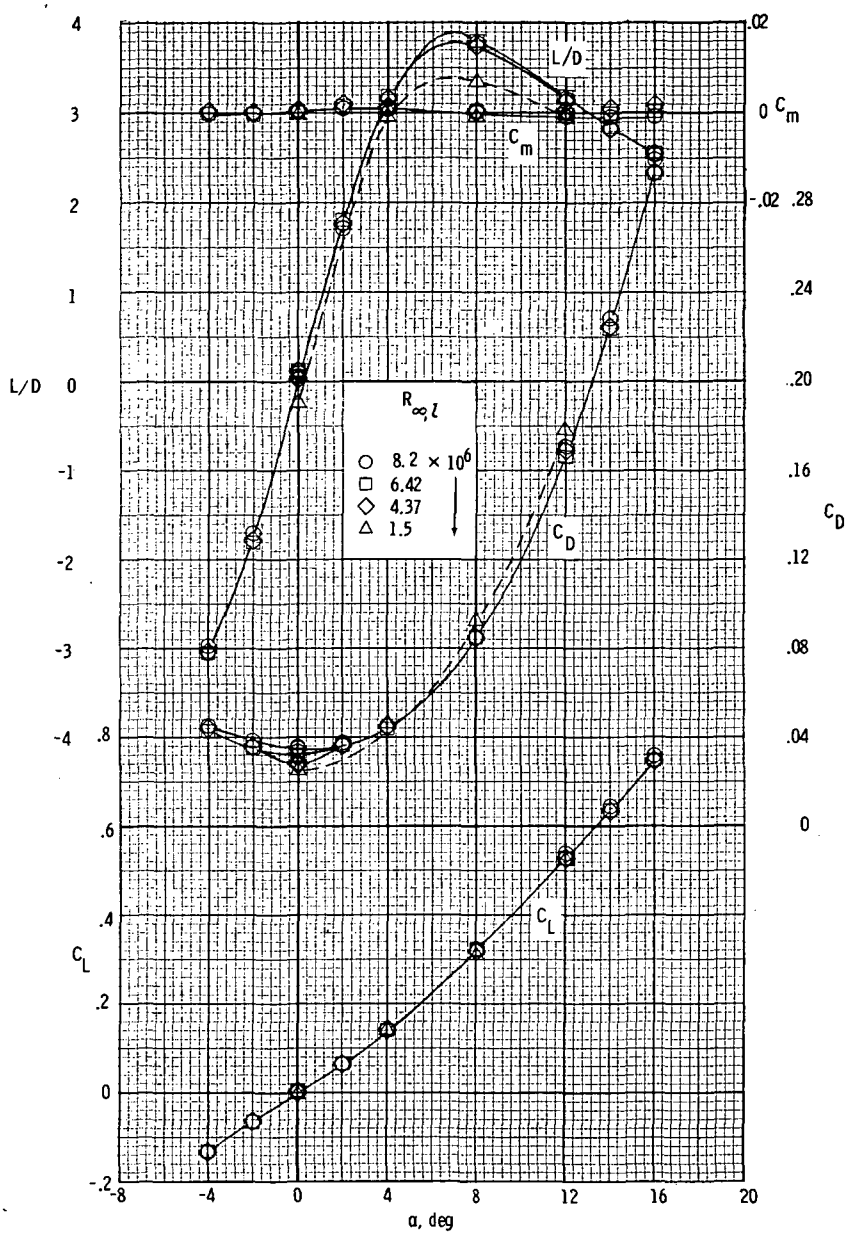

(f) n = 1.0.

Figure 3.- Concluded.

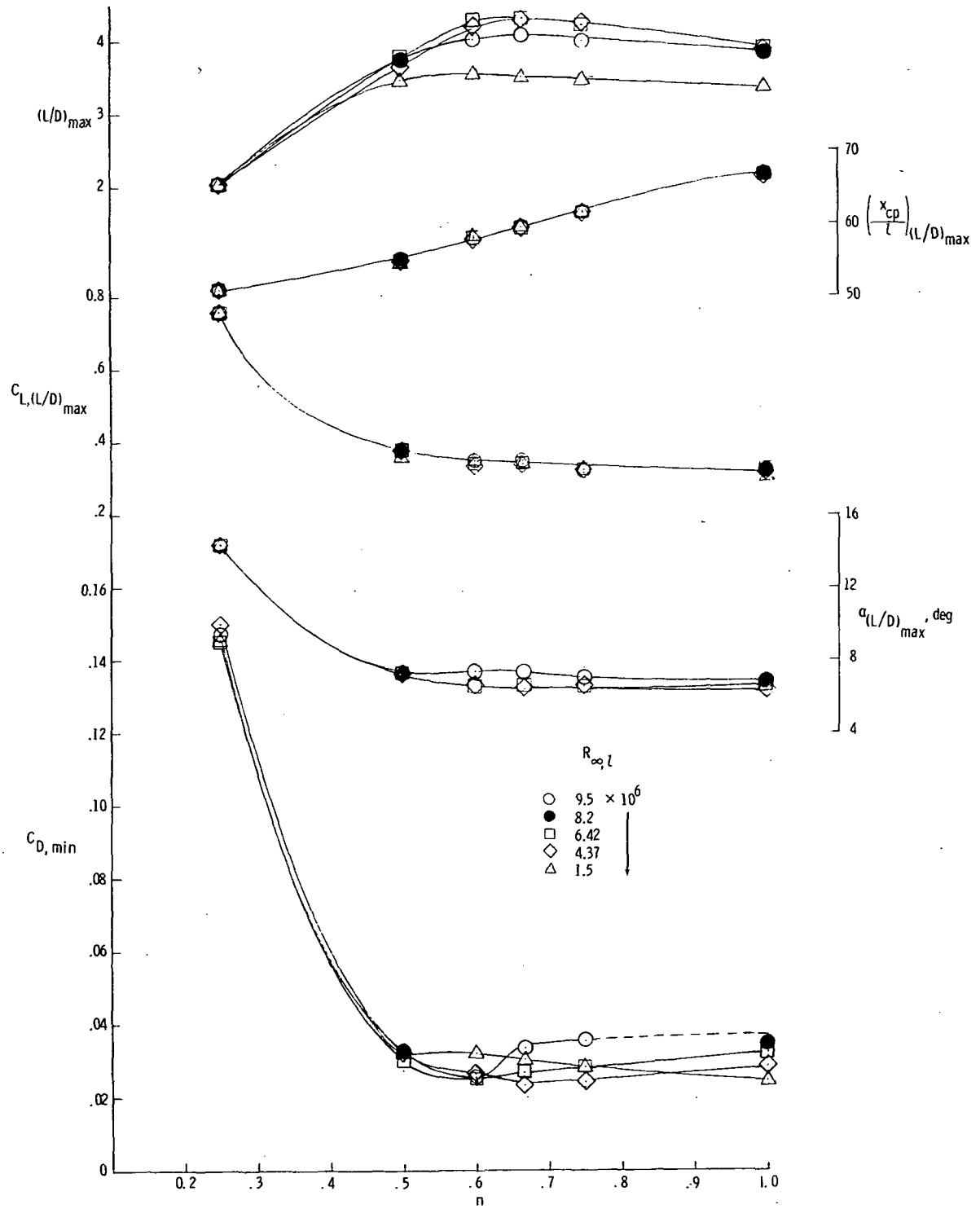

Figure 4.- Variation of measured aerodynamic performance with power-law exponent for fineness-ratio-6.63 power-law bodies at Mach number 6.

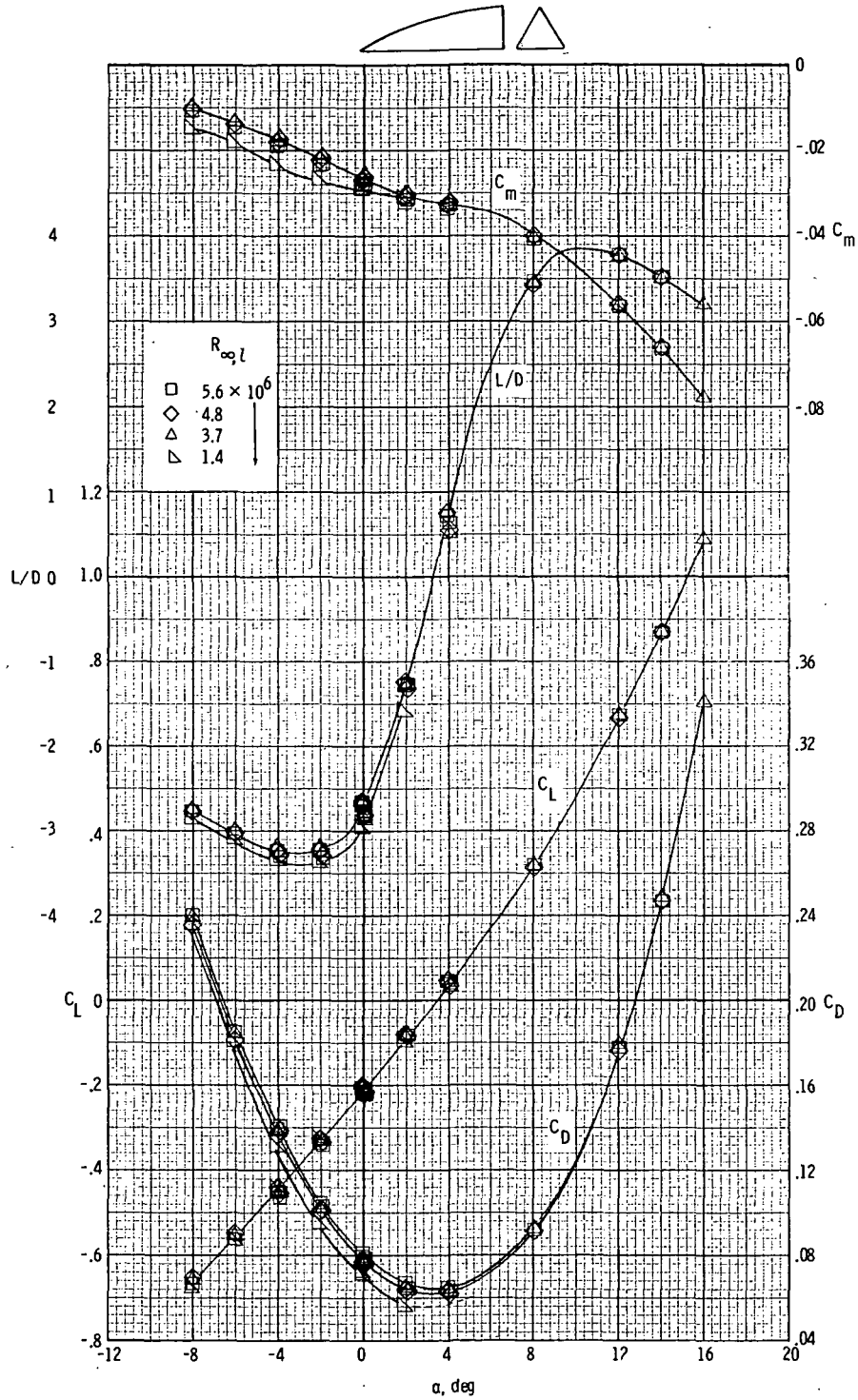

(a) Triangular cross section (body 1).

Figure 5.- Longitudinal aerodynamic characteristics of the polygonal bodies at Mach 6 and several Reynolds numbers.

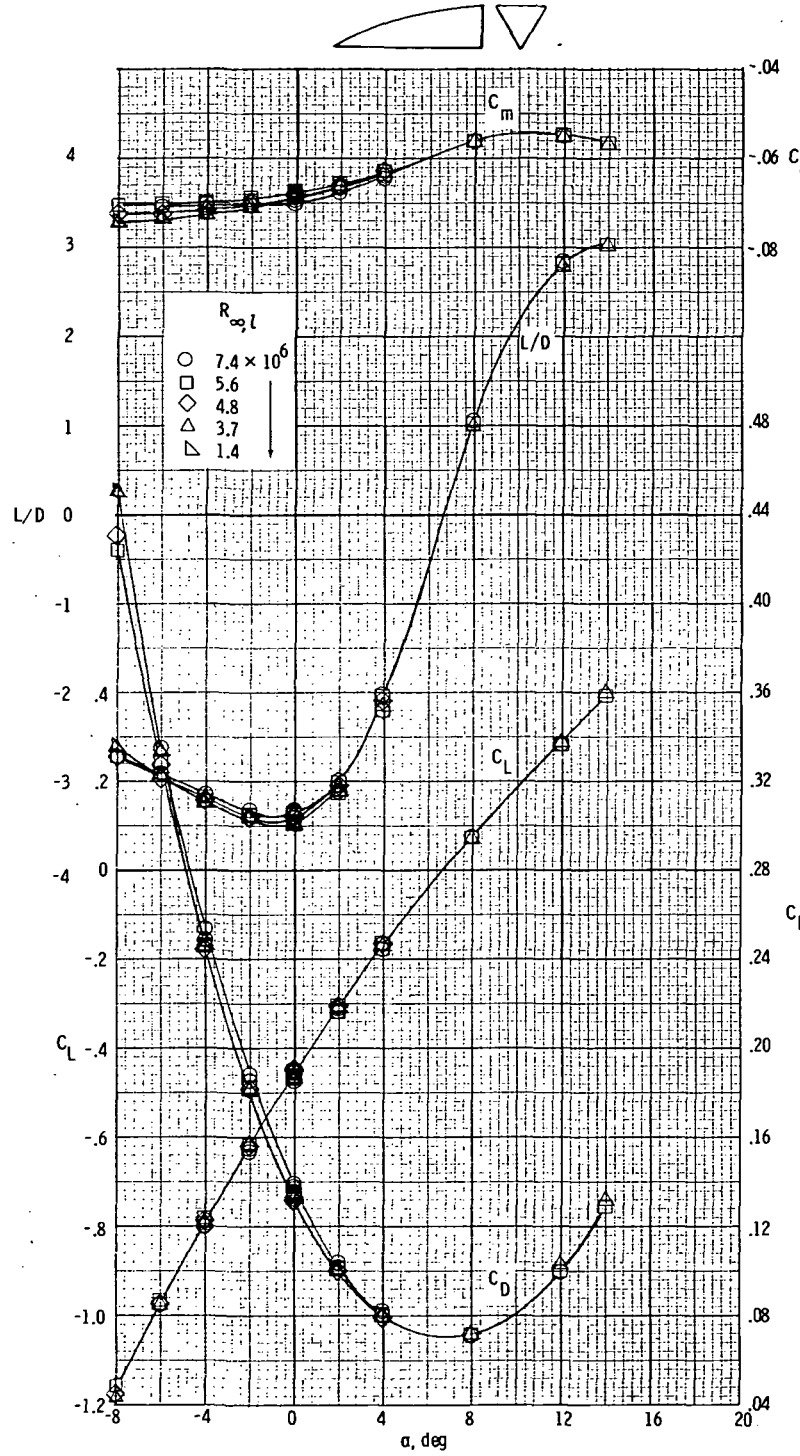

(b) Triangular cross section (body 2).

Figure 5.- Continued.

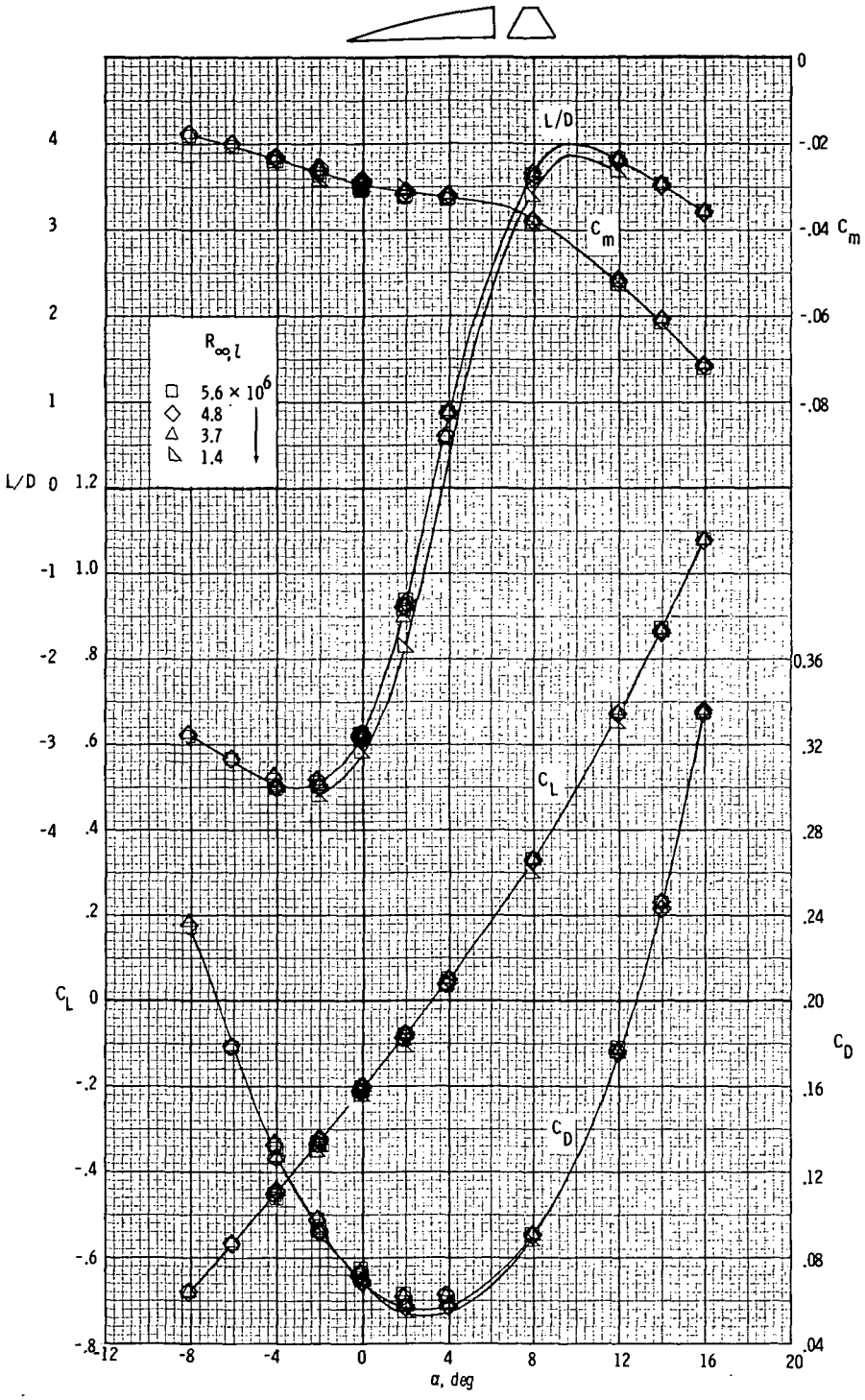

(c) Trapezoidal cross section (body 3). 1 to 3 top-to-bottom ratio.

Figure 5.- Continued.

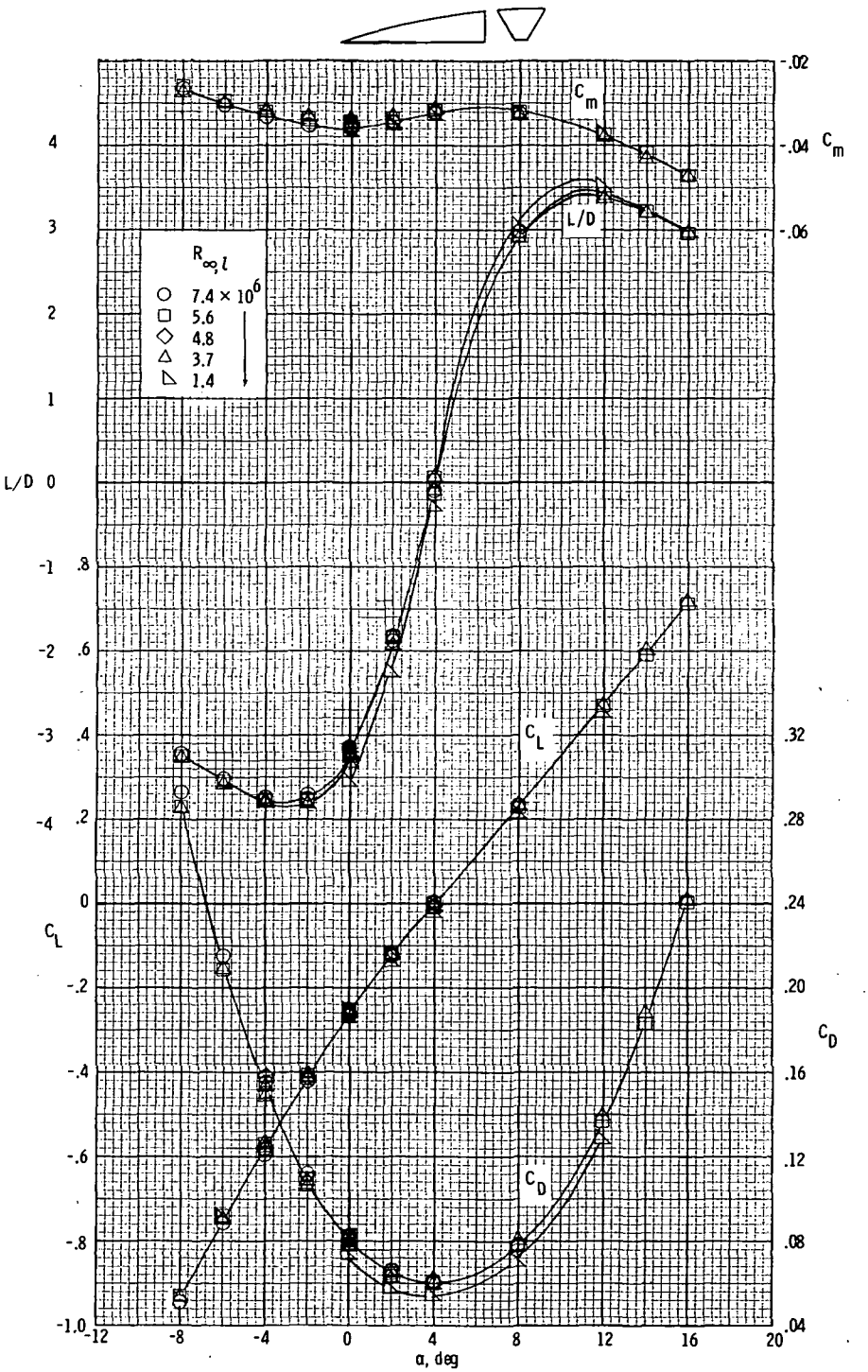

(d) Trapezoidal cross section (body 4). 1 to 3 bottom-to-top ratio.

Figure 5.- Continued.

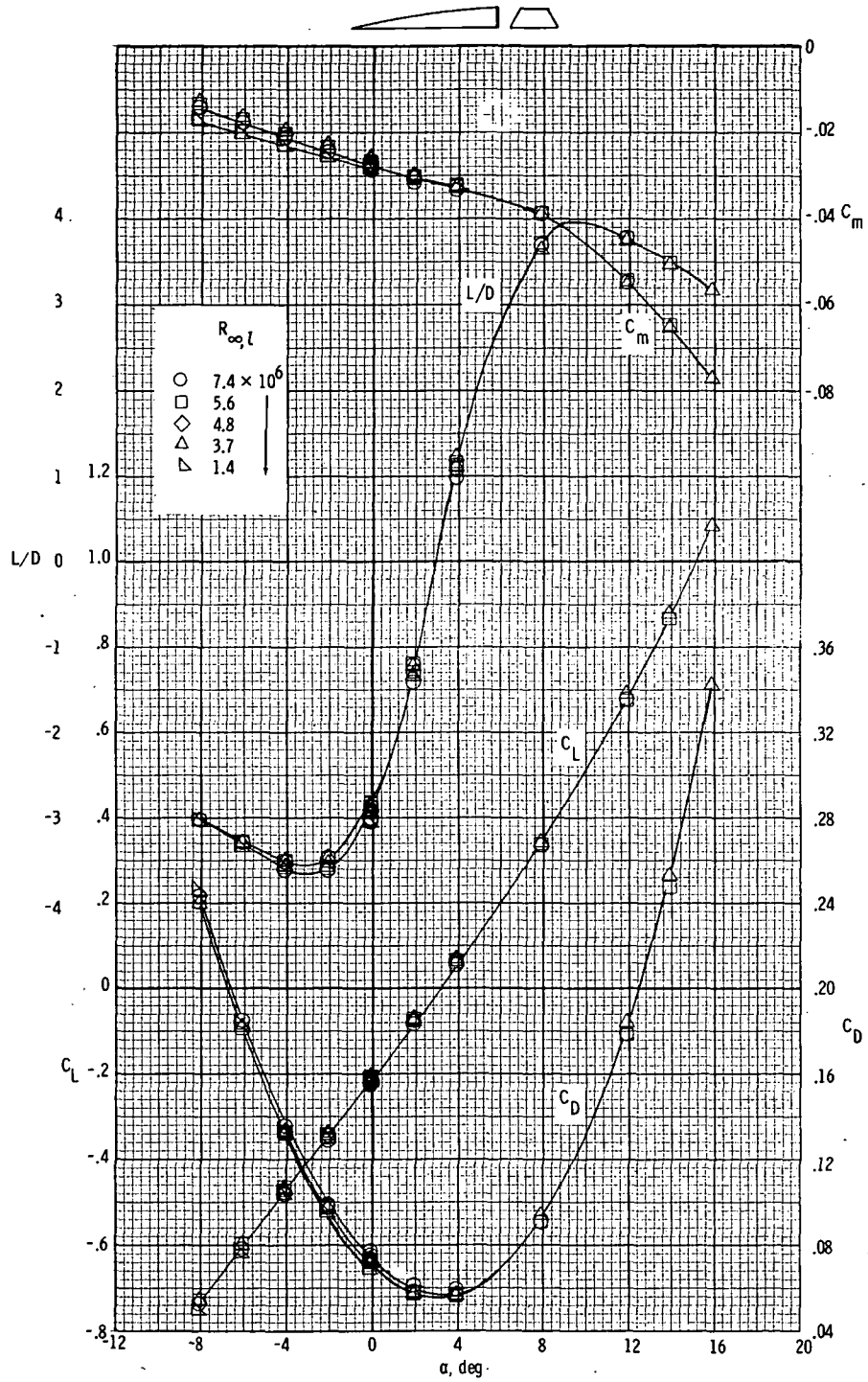

(e) Trapezoidal cross section (body 5). 2 to 3 top-to-bottom ratio.

Figure 5.- Continued.

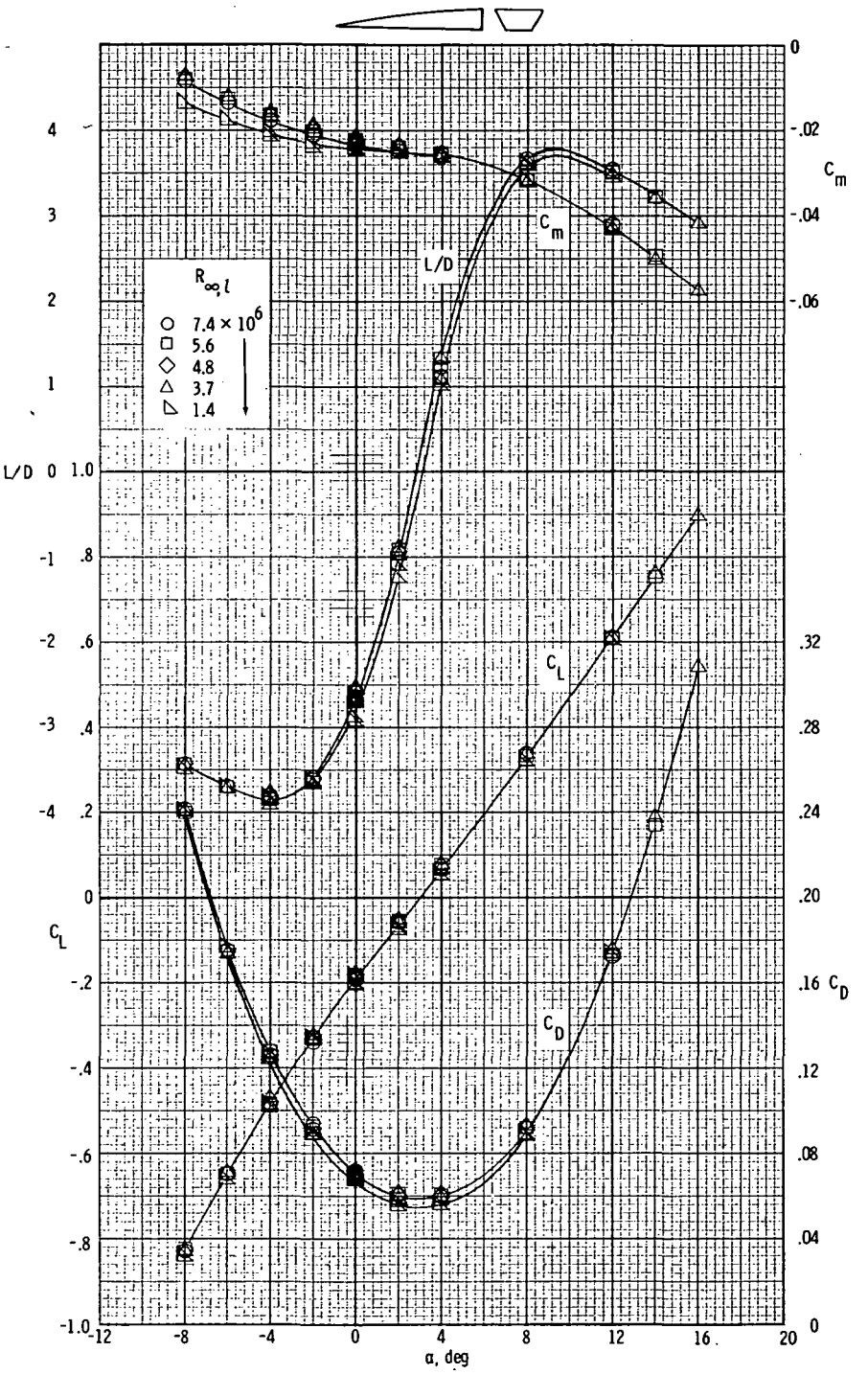

(f) Trapezoidal cross section (body 6). 2 to 3 bottom-to-top ratio.

Figure 5.- Continued.

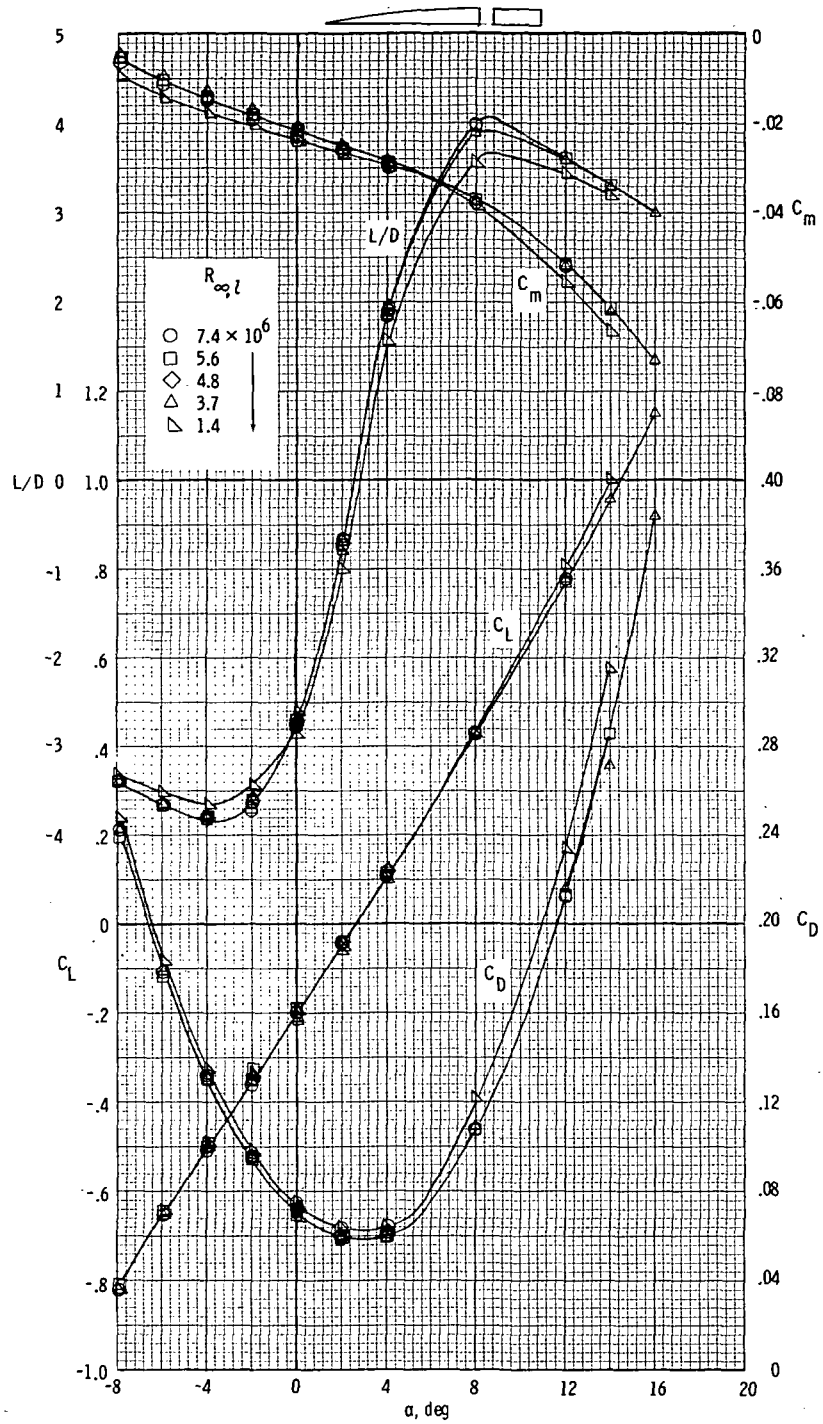

(g) Rectangular cross section, positive camber (body 7).

Figure 5. Concluded.

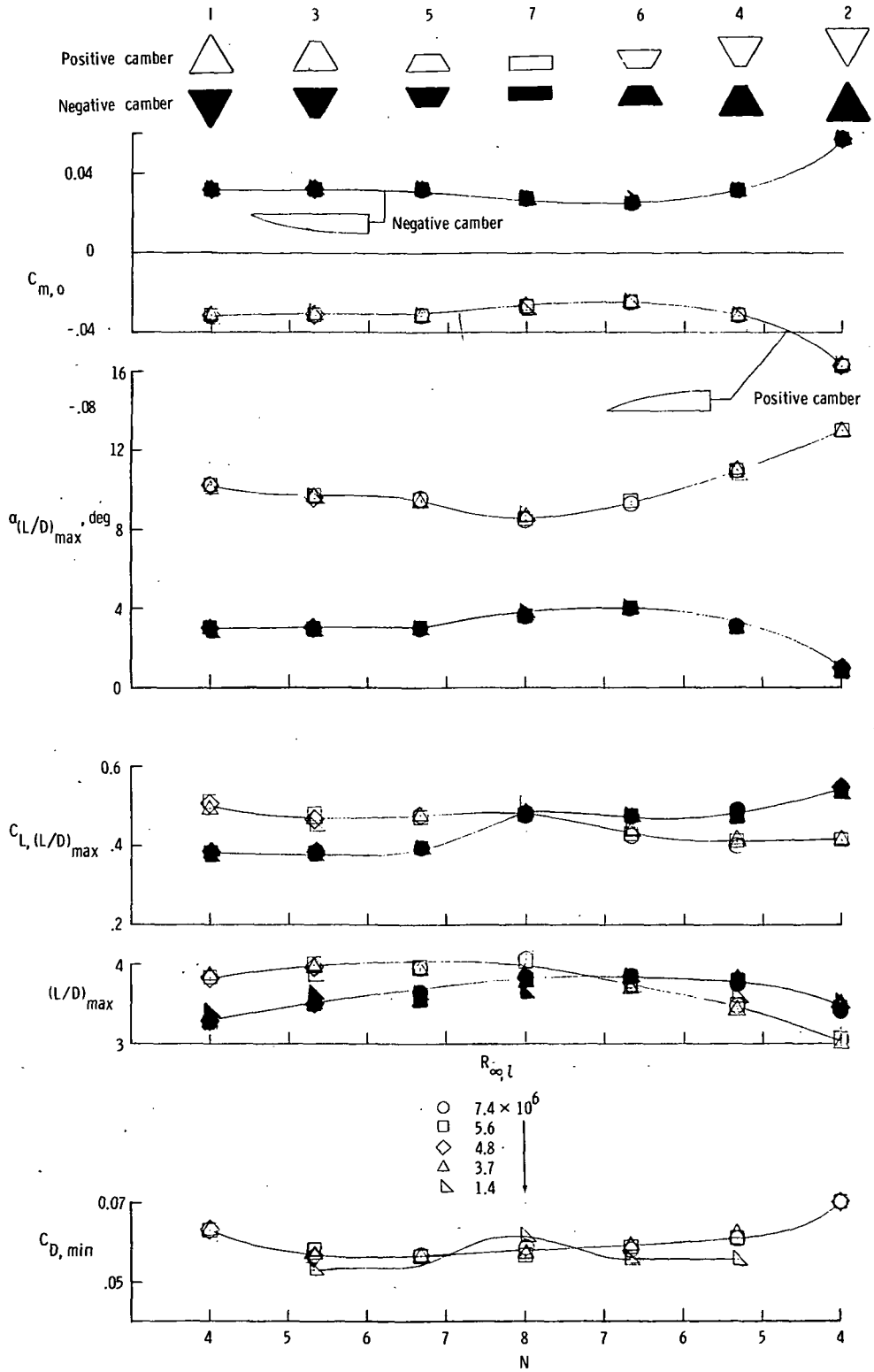

Figure 6.- Variation of measured aerodynamic performance with base span to height function for polygonal bodies. Solid symbols are for negative camber and open symbols are for positive camber.

"The aeronautical and space activities of the United States shall be conducted so as to contribute . . . to the expansion of human knowledge of phenomena in the atmosphere and space. The Administration shall provide for the widest practicable and appropriate dissemination of information concerning its activities and the results thereof."

—NATIONAL AERONAUTICS AND SPACE ACT OF 1958

NASA SCIENTIFIC AND TECHNICAL PUBLICATIONS

TECHNICAL REPORTS: Scientific and technical information considered important, complete, and a lasting contribution to existing knowledge.

TECHNICAL NOTES: Information less broad in scope but nevertheless of importance as a contribution to existing knowledge.

TECHNICAL MEMORANDUMS: Information receiving limited distribution because of preliminary data, security classification, or other reasons. Also includes conference proceedings with either limited or unlimited distribution.

CONTRACTOR REPORTS: Scientific and technical information generated under a NASA contract or grant and considered an important contribution to existing knowledge.

TECHNICAL TRANSLATIONS: Information published in a foreign language considered to merit NASA distribution in English.

SPECIAL PUBLICATIONS: Information derived from or of value to NASA activities. Publications include final reports of major projects, monographs, data compilations, handbooks, sourcebooks, and special bibliographies.

TECHNOLOGY UTILIZATION PUBLICATIONS: Information on technology used by NASA that may be of particular interest in commercial and other non-aerospace applications. Publications include Tech Briefs, Technology Utilization Reports and Technology Surveys.

Details on the availability of these publications may be obtained from:

SCIENTIFIC AND TECHNICAL INFORMATION OFFICE

NATIONAL AERONAUTICS AND SPACE ADMINISTRATION

Washington, D.C. 20546